# Study of the $e^+e^- \to K^+K^-$ reaction in the energy range from 2.6 to 8.0 GeV

J. P. Lees,[1] V. Poireau,[1] V. Tisserand,[1] E. Grauges,[2] A. Palano,[3a,3b] G. Eigen,[4] B. Stugu,[4] D. N. Brown,[5] L. T. Kerth,[5] Yu. G. Kolomensky,[5] M. J. Lee,[5] G. Lynch,[5] H. Koch,[6] T. Schroeder,[6] C. Hearty,[7] T. S. Mattison,[7] J. A. McKenna,[7] R. Y. So,[7] A. Khan,[8] V. E. Blinov,[9a,9b,9c] A. R. Buzykaev,[9a] V. P. Druzhinin,[9a,9b] V. B. Golubev,[9a,9b] E. A. Kravchenko,[9a,9b] A. P. Onuchin,[9a,9b,9c] S. I. Serednyakov,[9a,9b] Yu. I. Skovpen,[9a,9b] E. P. Solodov,[9a,9b] K. Yu. Todyshev,[9a,9b] A. J. Lankford,[10] B. Dey,[11] J. W. Gary,[11] O. Long,[11] M. Franco Sevilla,[12] T. M. Hong,[12] D. Kovalskyi,[12] J. D. Richman,[12] C. A. West,[12] A. M. Eisner,[13] W. S. Lockman,[13] W. Panduro Vazquez,[13] B. A. Schumm,[13] A. Seiden,[13] D. S. Chao,[14] C. H. Cheng,[14] B. Echenard,[14] K. T. Flood,[14] D. G. Hitlin,[14] J. Kim,[14] T. S. Miyashita,[14] P. Ongmongkolkul,[14] F. C. Porter,[14] M. Röhrken,[14] R. Andreassen,[15] Z. Huard,[15] B. T. Meadows,[15] B. G. Pushpawela,[15] M. D. Sokoloff,[15] L. Sun,[15] W. T. Ford,[16] J. G. Smith,[16] S. R. Wagner,[16] R. Ayad,[17,†] W. H. Toki,[17] B. Spaan,[18] D. Bernard,[19] M. Verderi,[19] S. Playfer,[20] D. Bettoni,[21a] C. Bozzi,[21a] R. Calabrese,[21a,21b] G. Cibinetto,[21a,21b] E. Fioravanti,[21a,21b] I. Garzia,[21a,21b] E. Luppi,[21a,21b] L. Piemontese,[21a] V. Santoro,[21a] A. Calcaterra,[22] R. de Sangro,[22] G. Finocchiaro,[22] S. Martellotti,[22] P. Patteri,[22] I. M. Peruzzi,[22] M. Piccolo,[22] A. Zallo,[22] R. Contri,[23a,23b] M. R. Monge,[23a,23b] S. Passaggio,[23a] C. Patrignani,[23a,23b] B. Bhuyan,[24] V. Prasad,[24] A. Adametz,[25] U. Uwer,[25] H. M. Lacker,[26] U. Mallik,[27] C. Chen,[28] J. Cochran,[28] S. Prell,[28] H. Ahmed,[29] A. V. Gritsan,[30] N. Arnaud,[31] M. Davier,[31] D. Derkach,[31] G. Grosdidier,[31] F. Le Diberder,[31] A. M. Lutz,[31] B. Malaescu,[31,‡] P. Roudeau,[31] A. Stocchi,[31] G. Wormser,[31] D. J. Lange,[32] D. M. Wright,[32] J. P. Coleman,[33] J. R. Fry,[33] E. Gabathuler,[33] D. E. Hutchcroft,[33] D. J. Payne,[33] C. Touramanis,[33] A. J. Bevan,[34] F. Di Lodovico,[34] R. Sacco,[34] G. Cowan,[35] D. N. Brown,[36] C. L. Davis,[36] A. G. Denig,[37] M. Fritsch,[37] W. Gradl,[37] K. Griessinger,[37] A. Hafner,[37] K. R. Schubert,[37] R. J. Barlow,[38,§] G. D. Lafferty,[38] R. Cenci,[39] B. Hamilton,[39] A. Jawahery,[39] D. A. Roberts,[39] R. Cowan,[40] R. Cheaib,[41] P. M. Patel,[41,*] S. H. Robertson,[41] N. Neri,[42a] F. Palombo,[42a,42b] L. Cremaldi,[43] R. Godang,[43,¶] D. J. Summers,[43] M. Simard,[44] P. Taras,[44] G. De Nardo,[45a,45b] G. Onorato,[45a,45b] C. Sciacca,[45a,45b] G. Raven,[46] C. P. Jessop,[47] J. M. LoSecco,[47] K. Honscheid,[48] R. Kass,[48] M. Margoni,[49a,49b] M. Morandin,[49a] M. Posocco,[49a] M. Rotondo,[49a] G. Simi,[49a,49b] F. Simonetto,[49a,49b] R. Stroili,[49a,49b] S. Akar,[50] E. Ben-Haim,[50] M. Bomben,[50] G. R. Bonneaud,[50] H. Briand,[50] G. Calderini,[50] J. Chauveau,[50] Ph. Leruste,[50] G. Marchiori,[50] J. Ocariz,[50] M. Biasini,[51a,51b] E. Manoni,[51a] A. Rossi,[51a] C. Angelini,[52a,52b] G. Batignani,[52a,52b] S. Bettarini,[52a,52b] M. Carpinelli,[52a,52b,**] G. Casarosa,[52a,52b] M. Chrzaszcz,[52a] F. Forti,[52a,52b] M. A. Giorgi,[52a,52b] A. Lusiani,[52a,52c] B. Oberhof,[52a,52b] E. Paoloni,[52a,52b] M. Rama,[52a] G. Rizzo,[52a,52b] J. J. Walsh,[52a] D. Lopes Pegna,[53] J. Olsen,[53] A. J. S. Smith,[53] F. Anulli,[54a] R. Faccini,[54a,54b] F. Ferrarotto,[54a] F. Ferroni,[54a,54b] M. Gaspero,[54a,54b] A. Pilloni,[54a,54b] G. Piredda,[54a] C. Bünger,[55] S. Dittrich,[55] O. Grünberg,[55] M. Hess,[55] T. Leddig,[55] C. Voß,[55] R. Waldi,[55] T. Adye,[56] E. O. Olaiya,[56] F. F. Wilson,[56] S. Emery,[57] G. Vasseur,[57] D. Aston,[58] D. J. Bard,[58] C. Cartaro,[58] M. R. Convery,[58] J. Dorfan,[58] G. P. Dubois-Felsmann,[58] M. Ebert,[58] R. C. Field,[58] B. G. Fulsom,[58] M. T. Graham,[58] C. Hast,[58] W. R. Innes,[58] P. Kim,[58] D. W. G. S. Leith,[58] S. Luitz,[58] V. Luth,[58] D. B. MacFarlane,[58] D. R. Muller,[58] H. Neal,[58] T. Pulliam,[58] B. N. Ratcliff,[58] A. Roodman,[58] R. H. Schindler,[58] A. Snyder,[58] D. Su,[58] M. K. Sullivan,[58] J. Va'vra,[58] W. J. Wisniewski,[58] H. W. Wulsin,[58] M. V. Purohit,[59] J. R. Wilson,[59] A. Randle-Conde,[60] S. J. Sekula,[60] M. Bellis,[61] P. R. Burchat,[61] E. M. T. Puccio,[61] M. S. Alam,[62] J. A. Ernst,[62] R. Gorodeisky,[63] N. Guttman,[63] D. R. Peimer,[63] A. Soffer,[63] S. M. Spanier,[64] J. L. Ritchie,[65] R. F. Schwitters,[65] J. M. Izen,[66] X. C. Lou,[66] F. Bianchi,[67a,67b] F. De Mori,[67a,67b] A. Filippi,[67a] D. Gamba,[67a,67b] L. Lanceri,[68a,68b] L. Vitale,[68a,68b] F. Martinez-Vidal,[69] A. Oyanguren,[69] J. Albert,[70] Sw. Banerjee,[70] A. Beaulieu,[70] F. U. Bernlochner,[70] H. H. F. Choi,[70] G. J. King,[70] R. Kowalewski,[70] M. J. Lewczuk,[70] T. Lueck,[70] I. M. Nugent,[70] J. M. Roney,[70] R. J. Sobie,[70] N. Tasneem,[70] T. J. Gershon,[71] P. F. Harrison,[71] T. E. Latham,[71] H. R. Band,[72] S. Dasu,[72] Y. Pan,[72] R. Prepost,[72] and S. L. Wu[72]

(The *BABAR* Collaboration)

[1]*Laboratoire d'Annecy-le-Vieux de Physique des Particules (LAPP), Université de Savoie, CNRS/IN2P3, F-74941 Annecy-Le-Vieux, France*
[2]*Universitat de Barcelona, Facultat de Fisica, Departament ECM, E-08028 Barcelona, Spain*
[3a]*INFN Sezione di Bari, I-70126 Bari, Italy*
[3b]*Dipartimento di Fisica, Università di Bari, I-70126 Bari, Italy*
[4]*University of Bergen, Institute of Physics, N-5007 Bergen, Norway*
[5]*Lawrence Berkeley National Laboratory and University of California, Berkeley, California 94720, USA*
[6]*Ruhr Universität Bochum, Institut für Experimentalphysik 1, D-44780 Bochum, Germany*
[7]*University of British Columbia, Vancouver, British Columbia, Canada V6T 1Z1*
[8]*Brunel University, Uxbridge, Middlesex UB8 3PH, United Kingdom*
[9a]*Budker Institute of Nuclear Physics SB RAS, Novosibirsk 630090, Russia*
[9b]*Novosibirsk State University, Novosibirsk 630090, Russia*
[9c]*Novosibirsk State Technical University, Novosibirsk 630092, Russia*
[10]*University of California at Irvine, Irvine, California 92697, USA*

 

[11]*University of California at Riverside, Riverside, California 92521, USA*
[12]*University of California at Santa Barbara, Santa Barbara, California 93106, USA*
[13]*University of California at Santa Cruz, Institute for Particle Physics, Santa Cruz, California 95064, USA*
[14]*California Institute of Technology, Pasadena, California 91125, USA*
[15]*University of Cincinnati, Cincinnati, Ohio 45221, USA*
[16]*University of Colorado, Boulder, Colorado 80309, USA*
[17]*Colorado State University, Fort Collins, Colorado 80523, USA*
[18]*Technische Universität Dortmund, Fakultät Physik, D-44221 Dortmund, Germany*
[19]*Laboratoire Leprince-Ringuet, Ecole Polytechnique, CNRS/IN2P3, F-91128 Palaiseau, France*
[20]*University of Edinburgh, Edinburgh EH9 3JZ, United Kingdom*
[21a]*INFN Sezione di Ferrara, I-44122 Ferrara, Italy*
[21b]*Dipartimento di Fisica e Scienze della Terra, Università di Ferrara, I-44122 Ferrara, Italy*
[22]*INFN Laboratori Nazionali di Frascati, I-00044 Frascati, Italy*
[23a]*INFN Sezione di Genova, I-16146 Genova, Italy*
[23b]*Dipartimento di Fisica, Università di Genova, I-16146 Genova, Italy*
[24]*Indian Institute of Technology Guwahati, Guwahati, Assam 781 039, India*
[25]*Universität Heidelberg, Physikalisches Institut, D-69120 Heidelberg, Germany*
[26]*Humboldt-Universität zu Berlin, Institut für Physik, D-12489 Berlin, Germany*
[27]*University of Iowa, Iowa City, Iowa 52242, USA*
[28]*Iowa State University, Ames, Iowa 50011-3160, USA*
[29]*Physics Department, Jazan University, Jazan 22822, Kingdom of Saudi Arabia*
[30]*Johns Hopkins University, Baltimore, Maryland 21218, USA*
[31]*Laboratoire de l'Accélérateur Linéaire, IN2P3/CNRS et Université Paris-Sud 11, Centre Scientifique d'Orsay, F-91898 Orsay Cedex, France*
[32]*Lawrence Livermore National Laboratory, Livermore, California 94550, USA*
[33]*University of Liverpool, Liverpool L69 7ZE, United Kingdom*
[34]*Queen Mary University of London, London E1 4NS, United Kingdom*
[35]*University of London, Royal Holloway and Bedford New College, Egham, Surrey TW20 0EX, United Kingdom*
[36]*University of Louisville, Louisville, Kentucky 40292, USA*
[37]*Johannes Gutenberg-Universität Mainz, Institut für Kernphysik, D-55099 Mainz, Germany*
[38]*University of Manchester, Manchester M13 9PL, United Kingdom*
[39]*University of Maryland, College Park, Maryland 20742, USA*
[40]*Massachusetts Institute of Technology, Laboratory for Nuclear Science, Cambridge, Massachusetts 02139, USA*
[41]*McGill University, Montréal, Québec, Canada H3A 2T8*
[42a]*INFN Sezione di Milano, I-20133 Milano, Italy*
[42b]*Dipartimento di Fisica, Università di Milano, I-20133 Milano, Italy*
[43]*University of Mississippi, University, Mississippi 38677, USA*
[44]*Université de Montréal, Physique des Particules, Montréal, Québec, Canada H3C 3J7*
[45a]*INFN Sezione di Napoli, I-80126 Napoli, Italy*
[45b]*Dipartimento di Scienze Fisiche, Università di Napoli Federico II, I-80126 Napoli, Italy*
[46]*NIKHEF, National Institute for Nuclear Physics and High Energy Physics, NL-1009 DB Amsterdam, Netherlands*
[47]*University of Notre Dame, Notre Dame, Indiana 46556, USA*
[48]*Ohio State University, Columbus, Ohio 43210, USA*
[49a]*INFN Sezione di Padova, I-35131 Padova, Italy*
[49b]*Dipartimento di Fisica, Università di Padova, I-35131 Padova, Italy*
[50]*Laboratoire de Physique Nucléaire et de Hautes Energies, IN2P3/CNRS, Université Pierre et Marie Curie-Paris6, Université Denis Diderot-Paris7, F-75252 Paris, France*
[51a]*INFN Sezione di Perugia, I-06123 Perugia, Italy*
[51b]*Dipartimento di Fisica, Università di Perugia, I-06123 Perugia, Italy*
[52a]*INFN Sezione di Pisa, I-56127 Pisa, Italy*
[52b]*Dipartimento di Fisica, Università di Pisa, I-56127 Pisa, Italy*
[52c]*Scuola Normale Superiore di Pisa, I-56127 Pisa, Italy*
[53]*Princeton University, Princeton, New Jersey 08544, USA*
[54a]*INFN Sezione di Roma, I-00185 Roma, Italy*
[54b]*Dipartimento di Fisica, Università di Roma La Sapienza, I-00185 Roma, Italy*
[55]*Universität Rostock, D-18051 Rostock, Germany*
[56]*Rutherford Appleton Laboratory, Chilton, Didcot, Oxon OX11 0QX, United Kingdom*

[57]CEA, Irfu, SPP, Centre de Saclay, F-91191 Gif-sur-Yvette, France
[58]SLAC National Accelerator Laboratory, Stanford, California 94309 USA
[59]University of South Carolina, Columbia, South Carolina 29208, USA
[60]Southern Methodist University, Dallas, Texas 75275, USA
[61]Stanford University, Stanford, California 94305-4060, USA
[62]State University of New York, Albany, New York 12222, USA
[63]Tel Aviv University, School of Physics and Astronomy, Tel Aviv 69978, Israel
[64]University of Tennessee, Knoxville, Tennessee 37996, USA
[65]University of Texas at Austin, Austin, Texas 78712, USA
[66]University of Texas at Dallas, Richardson, Texas 75083, USA
[67a]INFN Sezione di Torino, I-10125 Torino, Italy
[67b]Dipartimento di Fisica, Università di Torino, I-10125 Torino, Italy
[68a]INFN Sezione di Trieste, I-34127 Trieste, Italy
[68b]Dipartimento di Fisica, Università di Trieste, I-34127 Trieste, Italy
[69]IFIC, Universitat de Valencia-CSIC, E-46071 Valencia, Spain
[70]University of Victoria, Victoria, British Columbia, Canada V8W 3P6
[71]Department of Physics, University of Warwick, Coventry CV4 7AL, United Kingdom
[72]University of Wisconsin, Madison, Wisconsin 53706, USA
(Received 17 July 2015; published 20 October 2015)

The $e^+e^- \to K^+K^-$ cross section and charged-kaon electromagnetic form factor are measured in the $e^+e^-$ center-of-mass energy range ($E$) from 2.6 to 8.0 GeV using the initial-state radiation technique with an undetected photon. The study is performed using 469 fb$^{-1}$ of data collected with the *BABAR* detector at the PEP-II2 $e^+e^-$ collider at center-of-mass energies near 10.6 GeV. The form factor is found to decrease with energy faster than $1/E^2$ and approaches the asymptotic QCD prediction. Production of the $K^+K^-$ final state through the $J/\psi$ and $\psi(2S)$ intermediate states is observed. The results for the kaon form factor are used together with data from other experiments to perform a model-independent determination of the relative phases between electromagnetic (single-photon) and strong amplitudes in $J/\psi$ and $\psi(2S) \to K^+K^-$ decays. The values of the branching fractions measured in the reaction $e^+e^- \to K^+K^-$ are shifted relative to their true values due to interference between resonant and nonresonant amplitudes. The values of these shifts are determined to be about $\pm 5\%$ for the $J/\psi$ meson and $\pm 15\%$ for the $\psi(2S)$ meson.

DOI: 10.1103/PhysRevD.92.072008 PACS numbers: 13.66.Bc, 13.25.Gv, 13.40.Gp, 14.40.Df

## I. INTRODUCTION

The timelike charged-kaon form factor $F_K$ has been measured precisely in the threshold/$\phi$-meson region [1–3] and by several experiments [3–7] in the center-of-mass (c.m.) energy range 1.1–2.4 GeV, where substantial structure is evident. At higher energies, there are precise measurements at 3.671, [8], 3.772, and 4.170 GeV [9], and there is a scan that extends to 5 GeV [3]. The energy dependence of these higher-energy data is consistent with the asymptotic form predicted by perturbative quantum chromodynamics (pQCD), but their magnitude is about a factor of 4 higher than the predicted asymptotic value [10]

$$M^2_{K^+K^-}|F_K(M_{K^+K^-})| = 8\pi\alpha_s f_K^2, \quad (1)$$

where $M_{K^+K^-}$ is the $K^+K^-$ invariant mass, $\alpha_s$ is the strong coupling constant, and $f_K = 156.2 \pm 0.7$ MeV [[11] p. 1027] is the charged-kaon decay constant.[1] It is expected that the difference between the data and the asymptotic QCD prediction will decrease with increasing energy. Precise measurements at higher energies are needed to test this expectation.

In this paper we analyze the initial-state radiation (ISR) process $e^+e^- \to K^+K^-\gamma$. The $K^+K^-$ mass spectrum measured in this process is related to the cross section of the nonradiative process $e^+e^- \to K^+K^-$. Our previous measurement of $F_K$ [3] used the "large-angle" (LA) ISR technique, in which the radiated photon is detected and the $e^+e^- \to K^+K^-\gamma$ event is fully reconstructed. This gives good precision near threshold, but the cross section decreases rapidly with increasing energy, limiting that measurement to energies below 5 GeV. In this paper we

[*]Deceased.
[†]Now at University of Tabuk, Tabuk 71491, Saudi Arabia.
[‡]Now at Laboratoire de Physique Nucléaire et de Hautes Energies, IN2P3/CNRS, F-75252 Paris, France.
[§]Now at University of Huddersfield, Huddersfield HD1 3DH, UK.
[¶]Now at University of South Alabama, Mobile, Alabama 36688, USA.
[**]Also at Università di Sassari, I-07100 Sassari, Italy.

[1]We note that this value is larger by a factor of $\sqrt{2}$ than that used in Eq. (22) of Ref. [3].

utilize small-angle (SA) ISR events, in which the ISR photon is emitted close to the $e^+e^-$ collision axis and so is undetected. This allows us to perform an independent and complementary measurement of the charged-kaon form factor, which has better precision in the range 2.6–5 GeV, and extends the measurements up to 8 GeV.

The Born cross section for the ISR process integrated over the kaon momenta and the photon polar angle is

$$\frac{\mathrm{d}\sigma_{K^+K^-\gamma}(M_{K^+K^-})}{\mathrm{d}M_{K^+K^-}} = \frac{2M_{K^+K^-}}{s} W(s,x)\sigma_{K^+K^-}(M_{K^+K^-}), \quad (2)$$

where $s$ is the $e^+e^-$ c.m. energy squared, $x \equiv 2E^*_\gamma/\sqrt{s} = 1 - M^2_{K^+K^-}/s$, and $E^*_\gamma$ is the ISR photon energy in the $e^+e^-$ c.m. frame.[2] The function $W(s,x)$, describing the probability for single ISR emission at lowest order in quantum electrodynamics, is known to an accuracy better than 0.5% [12–14]. The $e^+e^- \to K^+K^-$ cross section is given in terms of the form factor by

$$\sigma_{K^+K^-}(M_{K^+K^-}) = \frac{\pi\alpha^2\beta^3 C}{3M^2_{K^+K^-}}|F_K(M_{K^+K^-})|^2, \quad (3)$$

where $\alpha$ is the fine-structure constant, $\beta = \sqrt{1-4m_K^2/M^2_{K^+K^-}}$, and $C$ is the final-state correction, which, in particular, takes into account extra photon radiation from the final state (see, e.g., Ref. [15]). In the mass region under study the factor $C$ is close to unity, and varies from 1.008 at 2.6 GeV/$c^2$ to 1.007 at 8 GeV/$c^2$.

In addition to the form factor, we measure the branching fractions for the decays $J/\psi \to K^+K^-$ and $\psi(2S) \to K^+K^-$. For the latter we study the interference between the resonant and nonresonant $e^+e^- \to K^+K^-$ amplitudes, and between the single-photon and strong $\psi \to K\bar{K}$ amplitudes (with $\psi = J/\psi, \psi(2S)$). As a result, we extract the interference corrections to the $J/\psi \to K^+K^-$ and $\psi(2S) \to K^+K^-$ branching fractions, which were not taken into account in previous measurements and determine the values of the phase difference between the single-photon and strong amplitudes in $J/\psi \to K\bar{K}$ and $\psi(2S) \to K\bar{K}$ decays. In contrast to previous determinations of this phase [16–18], we use a model-independent approach, calculating the single-photon decay amplitudes from our data on the charged-kaon form factor.

## II. THE *BABAR* DETECTOR, DATA, AND SIMULATED SAMPLES

We analyze a data sample corresponding to an integrated luminosity of 469 fb$^{-1}$ [19] recorded with the *BABAR* detector at the SLAC PEP-II2 asymmetric-energy (9-GeV $e^-$ and 3.1-GeV $e^+$) collider. About 90% of the data were collected at an $e^+e^-$ c.m. energy of 10.58 GeV (the $\Upsilon(4S)$ mass) and 10% at 10.54 GeV.

The *BABAR* detector is described in detail elsewhere [20]. Charged-particle tracking is provided by a five-layer silicon vertex tracker (SVT) and a 40-layer drift chamber (DCH), operating in the 1.5 T magnetic field of a superconducting solenoid. The position and energy of a photon-produced cluster are measured with a CsI(Tl) electromagnetic calorimeter (EMC). Charged-particle identification (PID) is provided by specific ionization ($\mathrm{d}E/\mathrm{d}x$) measurements in the SVT and DCH, and by an internally reflecting ring-imaging Cherenkov detector (DIRC). Muons are identified in the solenoid's instrumented flux return (IFR).

Simulated samples of signal events, and background $e^+e^- \to \pi^+\pi^-\gamma$ and $\mu^+\mu^-\gamma$ events, are generated with the Phokhara [21] Monte Carlo (MC) event generator, which takes into account next-to-leading-order radiative corrections. To obtain realistic estimates for the pion and kaon cross sections, the experimental values of the pion and kaon electromagnetic form factors measured in the CLEO experiment at $\sqrt{s} = 3.67$ GeV [8] are used in the event generator. The mass dependence of the form factors is assumed to be $1/m^2$, as predicted by asymptotic QCD [10]. The process $e^+e^- \to e^+e^-\gamma$ is simulated with the BHWIDE event generator [22].

Two-photon background from the process $e^+e^- \to e^+e^-K^+K^-$ is simulated with the GamGam event generator [23]. Background contributions from $e^+e^- \to q\bar{q}(\gamma_{\mathrm{ISR}})$, where $q$ represents a $u$, $d$, $s$ or $c$ quark, are simulated with the JETSET event generator [24].

The detector response is simulated using the Geant4 package [25]. The simulation takes into account the variations in the detector and beam-background conditions over the running period of the experiment.

## III. EVENT SELECTION

We select events with two tracks of opposite charge originating from the interaction region. The tracks must lie in the polar angle range $25.8° < \theta < 137.5°$ and be identified as kaons. The selected kaon candidates are fitted to a common vertex with a beam-spot constraint. The $\chi^2$ probability for this fit is required to be greater than 0.1%.

Conditions on the $K^+K^-$ transverse momentum ($p_{\mathrm{T},K^+K^-}$) and the missing-mass squared ($M^2_{\mathrm{miss}}$) recoiling against the $K^+K^-$ system are used for further selection. The $p_{\mathrm{T},K^+K^-}$ distribution for simulated $e^+e^- \to K^+K^-\gamma$ events is shown in Fig. 1. The peak near zero corresponds to ISR photons emitted along the collision axis, while the long tail is due to photons emitted at large angles. We apply the condition $p_{\mathrm{T},K^+K^-} < 0.15$ GeV/$c$, which removes large-angle ISR and suppresses backgrounds from $e^+e^- \to K^+K^-\pi^0$ and ISR processes with extra $\pi^0$ mesons.

[2]Throughout this paper, an asterisk denotes a quantity that is evaluated in the $e^+e^-$ c.m. frame, while quantities without asterisks are evaluated in the laboratory frame.

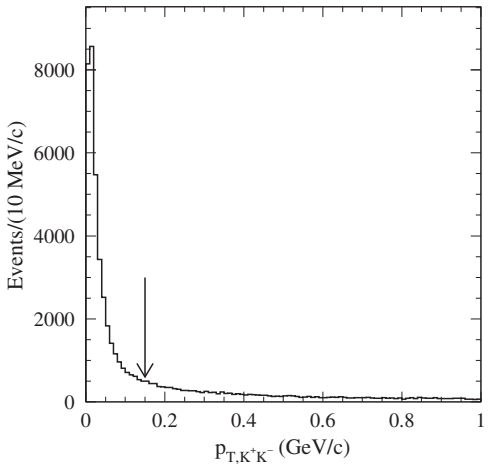


FIG. 1. The $p_{T,K^+K^-}$ distribution for simulated $e^+e^- \to K^+K^-\gamma$ events. The arrow indicates $p_{T,K^+K^-} = 0.15$ GeV/$c$.

The region of low $K^+K^-$ invariant mass cannot be studied with small-angle ISR due to limited detector acceptance. A $K^+K^-$ pair with $p_{T,K^+K^-} < 0.15$ GeV/$c$ is detected in *BABAR* when its invariant mass is larger than 2.5 (4.2) GeV/$c^2$ for an ISR photon emitted along the electron (positron) beam direction. The average values of the kaon momentum for the two photon directions are about 2.5 and 5 GeV/$c$, respectively. Since the probability for particle misidentification increases strongly with increasing momentum, we reject events with an ISR photon along the positron direction.

The $M^2_{\rm miss}$ distribution for simulated signal events is shown in Fig. 2. The signal distribution is peaked at zero, while the background distributions are shifted to negative values for $e^+e^- \to e^+e^-\gamma$ and $\mu^+\mu^-\gamma$ events and to positive values for $p\bar{p}\gamma$, two-photon and other ISR events. The condition $|M^2_{\rm miss}| < 1$ GeV$^2/c^4$ is applied to suppress background. Sideband regions in $M^2_{\rm miss}$ and $p_{T,K^+K^-}$ are

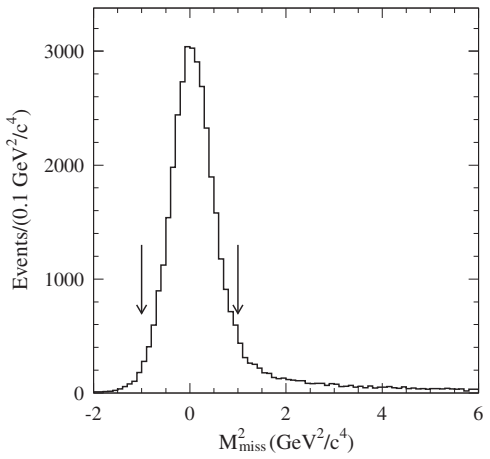


FIG. 2. The $M^2_{\rm miss}$ distribution for simulated $e^+e^- \to K^+K^-\gamma$ events. The arrows indicate $|M^2_{\rm miss}| = 1$ GeV$^2/c^4$.

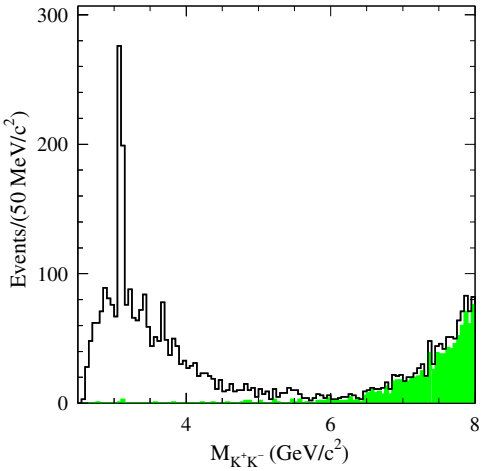


FIG. 3 (color online). The $K^+K^-$ mass spectrum for selected $K^+K^-\gamma$ candidates. The peaks near 3.1, 3.4, and 3.7 GeV/$c^2$ are from $J/\psi$, $\chi_{c0}$, and $\psi(2S)$ decays to $K^+K^-$, respectively. The shaded histogram shows events with at least one identified muon candidate.

used to estimate the remaining background from these sources, as described in Sec. IV.

The $K^+K^-$ invariant-mass spectrum for events selected with the criteria described above is shown in Fig. 3. A clear $J/\psi$ signal is seen in the spectrum, and there are also indications of small $\psi(2S)$ and $\chi_{c0}$ peaks. The $\chi_{c0}$ mesons are produced in the reaction $e^+e^- \to \psi(2S)\gamma \to \chi_{c0}\gamma\gamma$. The increase in the number of events for $M_{K^+K^-} > 6$ GeV/$c^2$ is due to background from the $e^+e^- \to \mu^+\mu^-\gamma$ process. To suppress the muon background, we apply the additional condition that neither kaon candidate be identified as a muon. Muon identification is based mainly on IFR information, and does not make use of the DIRC and d$E$/d$x$ measurements used for charged-kaon PID. For $\mu^+\mu^-\gamma$ background events, the probability for at least one of the charged particles to be identified as a muon is about 88% (see subsection IV A). The shaded histogram in Fig. 3 shows events with at least one identified muon candidate. The large muon background for larger values of $M_{K^+K^-}$ prevents us from providing results for $M_{K^+K^-} > 8$ GeV/$c^2$.

The mass spectrum with finer binning in the region of the charmonium resonances (3.0–4.5 GeV/$c^2$) is presented in the Supplemental Material [26], together with the mass resolution functions obtained from MC simulation with $M_{K^+K^-}$ near the $J/\psi$ and $\psi(2S)$ masses.

## IV. BACKGROUND ESTIMATION AND SUBTRACTION

Sources of background in the selected sample include the following: other two-body ISR processes $e^+e^- \to e^+e^-\gamma$, $\mu^+\mu^-\gamma$, $\pi^+\pi^-\gamma$, and $p\bar{p}\gamma$; ISR processes containing additional neutral particles, e.g., $e^+e^- \to K^+K^-\pi^0\gamma$ and $e^+e^- \to \psi(2S)\gamma \to \chi_{cJ}\gamma\gamma \to K^+K^-\gamma\gamma$; the two-photon

process $e^+e^- \to e^+e^-K^+K^-$; and nonradiative $e^+e^- \to q\bar{q}$ events containing a $K^+K^-$ pair plus neutrals, e.g., $e^+e^- \to K^+K^-\pi^0$. The background from the process $e^+e^- \to K^+K^-\pi^0$, which was dominant in our LA analysis [3], is strongly suppressed by the requirement on $p_{\mathrm{T},K^+K^-}$, and is found to be negligible in the SA analysis. The cross section for $e^+e^- \to p\bar{p}\gamma$ [27,28] is smaller than that for $e^+e^- \to K^+K^-\gamma$ in the mass region of interest, and this background is reduced to a negligible level by the requirement $|M^2_{\mathrm{miss}}| < 1\ \mathrm{GeV}^2/c^4$. The other categories of background are discussed in the following subsections.

### A. Background from $e^+e^- \to e^+e^-\gamma$, $\mu^+\mu^-\gamma$, and $\pi^+\pi^-\gamma$

To be selected and, thus, to represent background for this analysis, both final-state charged tracks in $e^+e^- \to e^+e^-\gamma$, $\mu^+\mu^-\gamma$, and $\pi^+\pi^-\gamma$ events must be misidentified as kaons, and the missing-mass squared must be poorly determined.

The probability to misidentify a pion as a kaon has been measured as a function of charge, momentum, and polar angle using a control sample of pions from $K_S \to \pi^+\pi^-$ decays. Using the measured misidentification probabilities, we calculate weights for simulated $e^+e^- \to \pi^+\pi^-\gamma$ events (see Sec. II) to be identified as $K^+K^-\gamma$ events and estimate a $\pi^+\pi^-\gamma$ background rate relative to the signal $K^+K^-\gamma$ rate ranging from $5 \times 10^{-5}$ at 3 GeV/$c^2$ to about $5 \times 10^{-3}$ at 7.5 GeV/$c^2$.

A similar approach is used to estimate the $e^+e^- \to e^+e^-\gamma$ background. The electron misidentification rate has been measured using $e^+e^- \to e^+e^-\gamma$ events with the photon detected at large angles. From MC simulation we estimate the electron contamination to be at most 0.5%. The PID requirements suppress $e^+e^- \to e^+e^-\gamma$ events by a factor of about $10^8$. We have verified this suppression by analyzing a sample of LA $K^+K^-\gamma$ candidates with the photon detected in the EMC. In this data sample, surviving $e^+e^- \to e^+e^-\gamma$ events can be identified by requiring a small opening angle between the photon direction and that of one of the charged-particle tracks.

In the subsequent analysis, we disregard possible backgrounds from $e^+e^-\gamma$ and $\pi^+\pi^-\gamma$ events since their contributions are expected to be negligible.

The $e^+e^- \to \mu^+\mu^-\gamma$ background is non-negligible for large values of $M_{K^+K^-}$. For $M_{K^+K^-} > 5.5\ \mathrm{GeV}/c^2$, we estimate the numbers of signal and background events in each of the five mass intervals listed in Table I by fitting the $M^2_{\mathrm{miss}}$ distributions in the range $[-2, +1]\ \mathrm{GeV}^2/c^4$, as shown in Fig. 4, using three components: signal events, the $\mu^+\mu^-\gamma$ background, and the ISR + two-photon background. The $M^2_{\mathrm{miss}}$ interval is extended to negative values to

TABLE I. The number of selected $K^+K^-$ candidates ($N_{\mathrm{data}}$), number of signal events ($N_{\mathrm{sig}}$), and estimated numbers of background events from $e^+e^- \to \mu^+\mu^-\gamma$ ($N_{\mu\mu\gamma}$), from the two-photon process $e^+e^- \to e^+e^-K^+K^-$ ($N_{\gamma\gamma}$), and from ISR processes with extra neutral particle(s) such as $e^+e^- \to K^+K^-\pi^0\gamma$ and $K^+K^-2\pi^0\gamma$ ($N_{\mathrm{ISR}}$). In the last column, $N_{\psi\chi}$ refers to the background from $J/\psi \to K^+K^-$ events for $3.0 < M_{K^+K^-} < 3.2\ \mathrm{GeV}/c^2$, from $\psi(2S) \to K^+K^-$ events for $3.6 < M_{K^+K^-} < 3.8\ \mathrm{GeV}/c^2$, and from $\psi(2S) \to \chi_{cJ}\gamma \to K^+K^-\gamma$ events for $3.2 < M_{K^+K^-} < 3.4$ and $3.4 < M_{K^+K^-} < 3.6\ \mathrm{GeV}/c^2$ (see Fig. 6). Events with $M_{K^+K^-} > 5.5\ \mathrm{GeV}/c^2$ are selected with the looser condition $-2 < M^2_{\mathrm{miss}} < 1\ \mathrm{GeV}^2/c^4$. For $N_{\mathrm{sig}}$, the first uncertainty is statistical and the second is systematic. For the numbers of background events, the combined uncertainty is quoted.

| $M_{K^+K^-}$ (GeV/$c^2$) | $N_{\mathrm{data}}$ | $N_{\mathrm{sig}}$ | $N_{\mu\mu\gamma}$ | $N_{\gamma\gamma}$ | $N_{\mathrm{ISR}}$ | $N_{\psi\chi}$ |
|---|---|---|---|---|---|---|
| 2.6–2.7 | 76 | $75 \pm 9 \pm 2$ | $< 0.1$ | $< 2$ | $0.6 \pm 0.5$ | – |
| 2.7–2.8 | 123 | $121 \pm 11 \pm 2$ | $< 0.1$ | $< 2$ | $1.6 \pm 1.0$ | – |
| 2.8–2.9 | 160 | $157 \pm 13 \pm 2$ | $< 0.1$ | $2.6 \pm 1.9$ | $0.9 \pm 0.7$ | – |
| 2.9–3.0 | 157 | $152 \pm 13 \pm 2$ | $< 0.1$ | $3.7 \pm 2.1$ | $1.3 \pm 0.9$ | – |
| 3.0–3.2 | 614 | $297 \pm 22 \pm 3$ | $< 0.1$ | $7.3 \pm 2.8$ | $2.3 \pm 1.6$ | $307.1 \pm 21.3$ |
| 3.2–3.4 | 290 | $279 \pm 17 \pm 2$ | $< 0.1$ | $5.1 \pm 2.1$ | $1.8 \pm 1.3$ | $4.6 \pm 1.6$ |
| 3.4–3.6 | 237 | $194 \pm 16 \pm 2$ | $< 0.1$ | $6.1 \pm 1.8$ | $3.1 \pm 2.0$ | $33.7 \pm 13.8$ |
| 3.6–3.8 | 212 | $162 \pm 16 \pm 1$ | $< 0.1$ | $3.2 \pm 0.9$ | $1.5 \pm 1.0$ | $45.8 \pm 11.0$ |
| 3.8–4.0 | 156 | $152 \pm 13 \pm 1$ | $< 0.1$ | $2.6 \pm 0.6$ | $1.4 \pm 1.0$ | – |
| 4.0–4.2 | 108 | $105 \pm 11 \pm 1$ | $< 0.1$ | $2.8 \pm 0.5$ | $0.3 \pm 0.4$ | – |
| 4.2–4.4 | 84 | $81 \pm 9 \pm 1$ | $0.2 \pm 0.1$ | $1.2 \pm 0.2$ | $1.7 \pm 1.0$ | – |
| 4.4–4.6 | 47 | $44.7 \pm 6.9 \pm 0.6$ | $0.1 \pm 0.1$ | $1.2 \pm 0.2$ | $1.0 \pm 0.7$ | – |
| 4.6–4.8 | 43 | $41.2 \pm 6.6 \pm 0.3$ | $0.1 \pm 0.1$ | $1.5 \pm 0.3$ | $0.2 \pm 0.3$ | – |
| 4.8–5.0 | 38 | $36.2 \pm 6.2 \pm 0.5$ | $0.5 \pm 0.3$ | $0.8 \pm 0.2$ | $0.5 \pm 0.4$ | – |
| 5.0–5.2 | 28 | $26.8 \pm 5.3 \pm 0.3$ | $0.2 \pm 0.1$ | $0.6 \pm 0.1$ | $0.4 \pm 0.4$ | – |
| 5.2–5.5 | 47 | $45.2 \pm 6.9 \pm 0.6$ | $0.9 \pm 0.5$ | $0.6 \pm 0.2$ | $0.3 \pm 0.3$ | – |
| 5.5–6.0 | 42 | $35.3 \pm 6.7 \pm 0.7$ | $6.0 \pm 3.7$ | $0.4 \pm 0.3$ | $0.7 \pm 0.5$ | – |
| 6.0–6.5 | 25 | $10.9 \pm 4.6 \pm 1.2$ | $11.4 \pm 4.3$ | $0.3 \pm 0.2$ | $2.0 \pm 1.1$ | – |
| 6.5–7.0 | 34 | $13.8 \pm 5.4 \pm 0.7$ | $18.5 \pm 5.6$ | $< 0.3$ | $0.8 \pm 0.6$ | – |
| 7.0–7.5 | 44 | $7.5 \pm 5.3 \pm 1.9$ | $33.3 \pm 6.9$ | $< 0.5$ | $3.4 \pm 1.8$ | – |
| 7.5–8.0 | 91 | $0.0 \pm 7.0 \pm 2.0$ | $87.6 \pm 10.5$ | $< 0.5$ | $3.5 \pm 1.9$ | – |

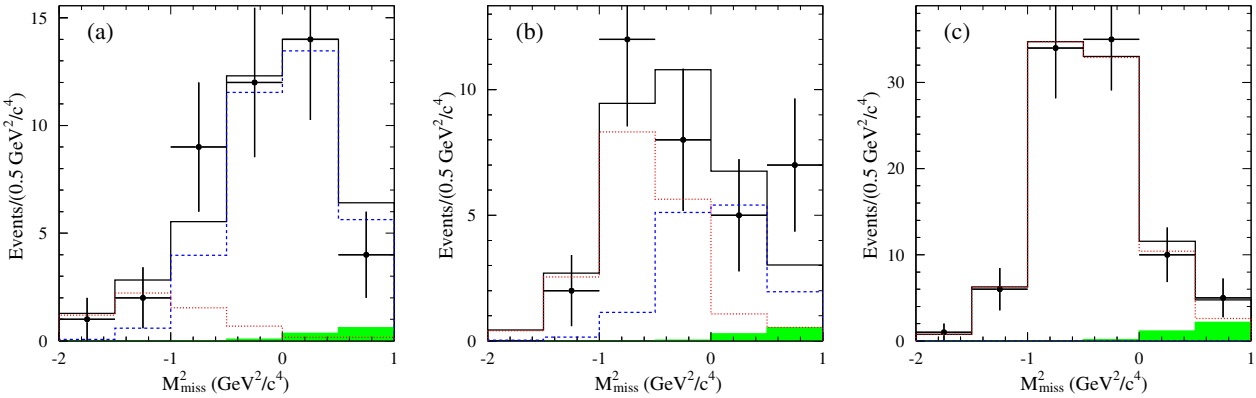


FIG. 4 (color online). The $M^2_{\rm miss}$ distributions for data (points with error bars) in three $M_{K^+K^-}$ intervals: (a) 5.5–6.0 GeV/$c^2$, (b) 6.5–7.0 GeV/$c^2$, and (c) 7.5–8.0 GeV/$c^2$. The solid histogram is the result of the fit described in the text. The dashed blue, dotted red, and shaded histograms show the contributions of signal, muon background, and ISR + two-photon background, respectively.

increase the sensitivity to $e^+e^- \to \mu^+\mu^-\gamma$ background and thus to better determine its contribution. The distribution for signal events is taken from simulation and is centered at zero. The distribution for the $\mu^+\mu^-\gamma$ background is obtained using data events with at least one identified muon, and is shifted to negative $M^2_{\rm miss}$ values because of the muon-kaon mass difference. We also include the small contributions from ISR and two-photon events estimated as described below in Secs. IV B and IV C. The fitted parameters are the numbers of signal ($N_{\rm sig}$) and muon-background ($N_{\mu\mu\gamma}$) events.

The results of the fits are listed in the last five rows of Table I and are shown in Fig. 4 for three representative intervals of $M_{K^+K^-}$. The first uncertainty in $N_{\rm sig}$ is statistical, while the second, systematic, uncertainty, accounts for the uncertainty in the numbers of ISR and two-photon background events. The $N_{\rm sig}$ results in Table I for $M_{K^+K^-} > 5.5$ GeV/$c^2$ are obtained with the condition $-2 < M^2_{\rm miss} < 1$ GeV$^2/c^4$. They can be scaled into our standard selection $|M^2_{\rm miss}| < 1$ GeV$^2/c^4$ by multiplying the results in the 5.5–6.5 GeV/$c^2$ and 6.5–7.5 GeV/$c^2$ mass ranges by 0.98 and 0.99, respectively. For $M_{K^+K^-} >$ 7.5 GeV/$c^2$ the scaling factor is consistent with 1.0. The scale factors are determined using simulated signal events.

Below 5.5 GeV/$c^2$, where the muon background is small, we adopt a simpler approach and estimate the number of $\mu^+\mu^-\gamma$ background events in each mass interval using the number of selected events $N_{1\mu}$ with at least one charged track identified as a muon. The number of background events is estimated as

$$N_{\mu\mu\gamma} = C_\mu(N_{1\mu} - k_{1\mu}N_{\rm data}), \qquad (4)$$

where $C_\mu$, evaluated as described below, is the ratio of the number of selected $\mu^+\mu^-\gamma$ events with no identified muon to the number of events with at least one identified muon, $k_{1\mu}$ is the fraction of selected $K^+K^-\gamma$ events with at least one identified muon, and $N_{\rm data}$ is the number of events in the respective $M_{K^+K^-}$ interval. The value of $k_{1\mu}$ is taken from simulated signal events and varies from 0.006 at $M_{K^+K^-} = 2.6$ GeV/$c^2$ to 0.01 at $M_{K^+K^-} = 5.5$ GeV/$c^2$.

Very few simulated $\mu^+\mu^-\gamma$ events have both tracks identified as kaons and neither identified as a muon, so $C_\mu$ is studied as a function of $M_{K^+K^-}$ using the probability for an individual muon to be identified as both a kaon and a muon, assuming the probabilities for the two tracks to be independent. We find that $C_\mu$ does not exhibit a significant dependence on mass within the range of our measurements, 2.6–8.0 GeV/$c^2$. Therefore, $C_\mu$ used in Eq. (4) is estimated from the fitted numbers of $\mu^+\mu^-\gamma$ events above 5.5 GeV/$c^2$. We find $C_\mu = 0.14 \pm 0.01 \pm 0.08$, where the first uncertainty is from the fits and the second accounts for the full range of values in different mass intervals in data and simulation (for purposes of information, the MC result is $C_\mu = 0.11$). The resulting estimated numbers of $\mu^+\mu^-\gamma$ background events are listed in Table I. For masses below 4.2 GeV/$c^2$, $(N_{1\mu} - k_{1\mu}N_{\rm data})$ is consistent with zero, and we take 0.1 as both an upper limit and uncertainty.

### B. Multibody ISR background

Background ISR events containing a $K^+K^-$ pair and one or more $\pi^0$ and/or $\eta$ mesons are distinguishable by their nonzero values of $M^2_{\rm miss}$ and $p_{{\rm T},K^+K^-}$, but some events with a small number of neutral particles still can enter the selected data sample. Figure 5(a) shows the two-dimensional distribution of $M^2_{\rm miss}$ versus $p_{{\rm T},K^+K^-}$ for data events before the requirements on these two variables, indicated by the lines, are applied. The bottom left rectangle is the signal region. The same distribution for simulated signal events is shown in Fig. 5(b), and is similar in structure except for a deficit in the upper right rectangle, which we take as a sideband region. The distribution for ISR background events produced by JETSET is shown in Fig. 5(c). It should be noted that most (98%) simulated

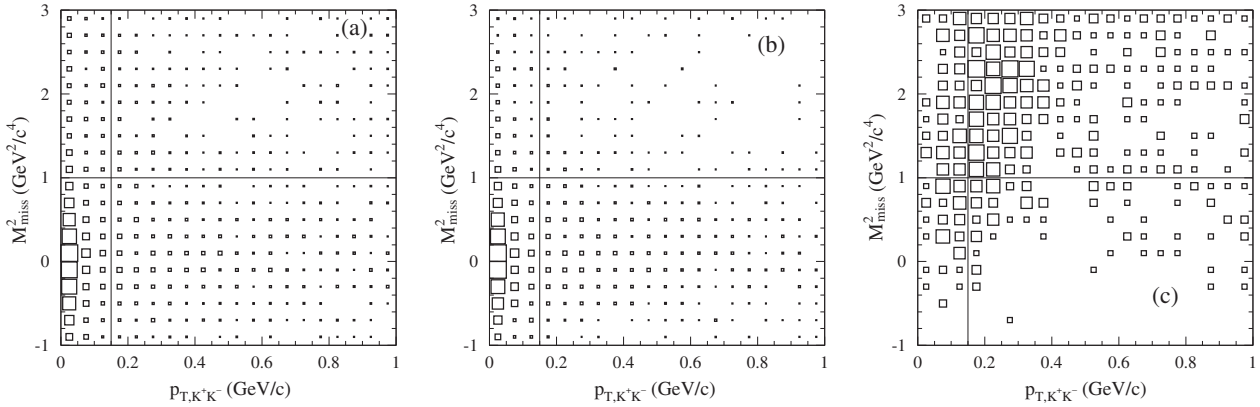


FIG. 5. The distributions of $M^2_{\rm miss}$ versus $p_{{\rm T},K^+K^-}$ for (a) data events, (b) simulated signal events, and (c) simulated ISR background events. Events in the $J/\psi$ and $\chi_{c0}$ mass regions, $3.05 < M_{K^+K^-} < 3.15$ GeV$/c^2$ and $3.38 < M_{K^+K^-} < 3.46$ GeV$/c^2$, are excluded from the distributions; regions near the $\chi_{c2}$ and $\psi(2S)$ are not excluded, since their signal content is quite small. The lines indicate the boundaries of the signal region (bottom left rectangle) and the sideband region (top right rectangle).

background events in the signal region are from the process $e^+e^- \to K^+K^-\pi^0\gamma$, while the fraction in the sideband region is about 80%.

The number of data events in the sideband region $N_2$ is used to estimate the ISR background in the signal region using

$$N_{\rm ISR} = \frac{N_2 - \beta_{\rm sig} N_1}{\beta_{\rm bkg} - \beta_{\rm sig}}, \tag{5}$$

where $N_1$ is the number of data events in the signal region, and $\beta_{\rm sig}$ and $\beta_{\rm bkg}$ are the $N_2/N_1$ ratios from signal and background simulation, respectively. The coefficient $\beta_{\rm sig}$ increases linearly from $0.046 \pm 0.005$ at $M_{K^+K^-} = 2.6$ GeV$/c^2$ to $0.074 \pm 0.005$ at 8.0 GeV$/c^2$, where the uncertainty is statistical, whereas $\beta_{\rm bkg} = 7.6 \pm 1.0 \pm 4.0$ is independent of $M_{K^+K^-}$. The first uncertainty in $\beta_{\rm bkg}$ is statistical, and the second is systematic. The latter takes into account possible differences between data and simulation in the background composition, and in the kinematic distributions of $e^+e^- \to K^+K^-\pi^0\gamma$ events.

The regions 3.0–3.2 and 3.6–3.8 GeV$/c^2$ contain resonant contributions from the decays $J/\psi \to K^+K^-$ and $\psi(2S) \to K^+K^-$, respectively. The resonant and nonresonant contributions are determined by the fits described in Sec. VII, and such fits are also applied to the sideband regions. The resulting numbers of nonresonant events, $N_1$ and $N_2$, are used to estimate the ISR background.

Similarly, the $M_{K^+K^-}$ regions 3.2–3.4 and 3.4–3.6 GeV$/c^2$ contain $\chi_{c0}$ and $\chi_{c2}$ decays, as seen in Fig. 6. The $\chi_{cJ}$ states are produced in the reaction $e^+e^- \to \psi(2S)\gamma$, followed by $\psi(2S) \to \chi_{cJ}\gamma$. A similar set of fits is used to determine $N_1$, $N_2$, and the background contribution from the $\chi_{cJ}$ states, and the fit results are shown in Fig. 6. The estimated numbers of ISR background events are listed in Table I along with the fitted numbers of $\psi$ and $\chi_{cJ}$ decays in the relevant mass intervals.

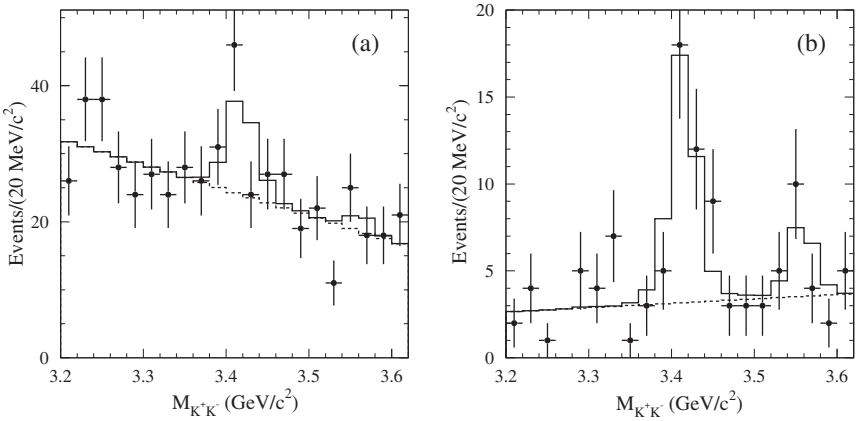


FIG. 6. The $M_{K^+K^-}$ spectra for data (points with error bars) in the vicinity of the $\chi_{c0}$ and $\chi_{c2}$ resonances for the $M^2_{\rm miss}$–$p_{{\rm T},K^+K^-}$ (a) signal region and (b) sideband region. The solid histograms result from the fits described in the text. The dashed histograms represent the nonresonant contributions.

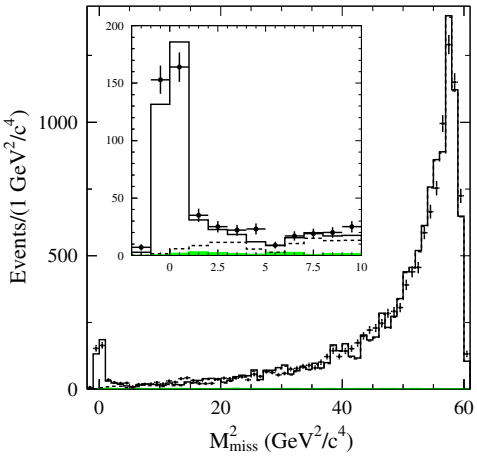


FIG. 7 (color online). The $M^2_{\rm miss}$ distribution for data (points with error bars) with $2.8 < M_{K^+K^-} < 3.0$ GeV/$c^2$ selected with all the criteria described in Sec. III except for the requirement $|M^2_{\rm miss}| < 1$ GeV$^2/c^4$. The solid histogram is a sum of signal and background distributions obtained from MC simulation. The dashed histogram shows the distribution for two-photon events, and the shaded (almost invisible) histogram shows the small contribution of all other background processes. The inset shows an enlarged view of the region $-2 < M^2_{\rm miss} < 10$ GeV$^2/c^4$. Above 10 GeV$^2/c^4$ the solid and dashed histograms are indistinguishable.

### C. Two-photon background

Two-photon events corresponding to the process $e^+e^- \to e^+e^-\gamma^*\gamma^* \to e^+e^-K^+K^-$ are distinguished by their larger values of $M^2_{\rm miss}$. Figure 7 shows the $M^2_{\rm miss}$ distribution for data events in the range $2.8 < M_{K^+K^-} < 3.0$ GeV/$c^2$ that satisfy all the criteria in Sec. III except for that on $M^2_{\rm miss}$. The two-photon events, which dominate the large $|M^2_{\rm miss}|$ region, are generally seen to be well separated from signal events but to nonetheless have a tail that extends into the signal region $|M^2_{\rm miss}| < 1$ GeV$^2/c^4$. The exact shape of this tail depends on the unknown kaon angular distribution. Therefore, we reweight our simulation (generated with a uniform distribution) to reproduce the $\cos\theta_K$ distribution observed in the data in each $M_{K^+K^-}$ interval; here $\theta_K$ is the angle between the $K^+$ momentum in the $K^+K^-$ rest frame and the $e^-$ beam direction in the $e^+e^-$ c.m. frame. The data and reweighted simulated $\cos\theta_K$ distributions are compared in Fig. 8. The simulated $M^2_{\rm miss}$ distribution is shown in Fig. 7, where it is seen to reproduce the data well.

The two-photon background in each $M_{K^+K^-}$ interval is estimated from the number of data events with $M^2_{\rm miss} > d$ and a scale factor from the simulation. The $M^2_{\rm miss}$ distribution changes with $M_{K^+K^-}$, and the value of $d$ is 20 GeV$^2/c^4$ for $M_{K^+K^-} < 4.4$ GeV/$c^2$, 10 GeV$^2/c^4$ for $M_{K^+K^-} > 6.5$ GeV/$c^2$, and varies linearly in-between. The scale factor ranges from $10^{-4}$ in the 2.6–2.7 GeV/$c^2$ interval to about $10^{-2}$ in the 7.0–7.5 GeV/$c^2$ interval. However, the number of two-photon events decreases with increasing $M_{K^+K^-}$. The estimated background event contributions are listed in Table I.

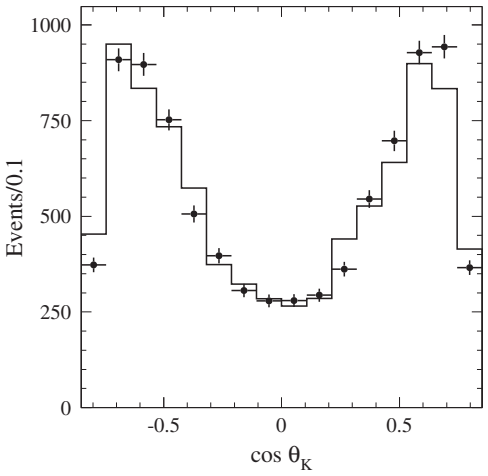


FIG. 8. The $\cos\theta_K$ distribution for data (points with error bars) and reweighted simulated events (histogram) with $M^2_{\rm miss} > 20$ GeV$^2/c^4$ from the $K^+K^-$ mass range 2.8–3.0 GeV/$c^2$.

The numbers of signal events obtained after background subtraction are listed in Table I. The first uncertainty in $N_{\rm sig}$ is statistical and the second is systematic. The systematic term accounts for the uncertainties in the numbers of $e^+e^- \to \mu^+\mu^-\gamma$ and two-photon background events, and the uncertainties in the coefficients $\beta_{\rm sig}$ and $\beta_{\rm bkg}$ in the ISR background subtraction procedure.

## V. DETECTION EFFICIENCY

The detection efficiency, $\varepsilon_{\rm MC}$, determined using MC simulation, is shown in Fig. 9 as a function of $M_{K^+K^-}$. The nonmonotonic behavior observed for $M_{K^+K^-} > 5.5$ GeV/$c^2$ is introduced by filters designed to reduce background before the event-reconstruction stage.

Corrections are applied to $\varepsilon_{\rm MC}$ to account for data-MC simulation differences in detector response

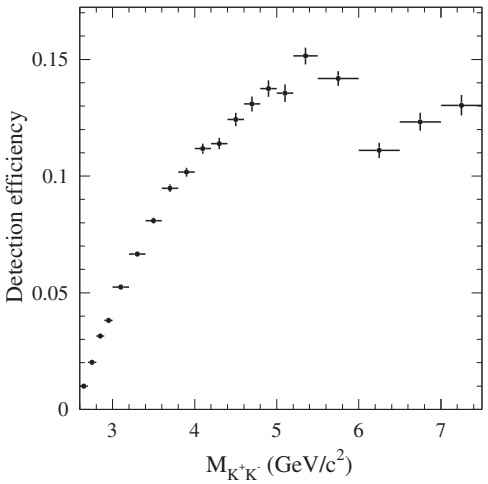


FIG. 9. The $K^+K^-$ mass dependence of the detection efficiency for simulated $e^+e^- \to K^+K^-\gamma$ events.

TABLE II. Values of the efficiency corrections, $\delta_i$. The three values in the rows "PID" and "total" correspond to $M_{K^+K^-} = 2.6$, 6.0, and 7.5 GeV/$c^2$, respectively.

| Effect | $\delta_i$ (%) |
|---|---|
| Trigger | $-1.0 \pm 0.5$ |
| PID | $-2.0 \pm 0.4/-4.0 \pm 0.5/-10.0 \pm 1.7$ |
| Track reconstruction | $0.0 \pm 1.6$ |
| Requirements on $p_{T,K^+K^-}$ and $M^2_{\rm miss}$ | $0.0 \pm 1.5$ |
| Total | $-3.0 \pm 2.3/-5.0 \pm 2.3/-11.0 \pm 2.8$ |

$$\varepsilon = \varepsilon_{\rm MC} \prod_{i=1}^{4} (1 + \delta_i), \tag{6}$$

where the $\delta_i$ terms are the efficiency corrections listed in Table II. The difference between data and simulation in trigger efficiency is studied using the overlap of the samples of events satisfying two independent sets of trigger criteria based on signals from the EMC and DCH. The correction for trigger inefficiency is found to be $(-1.0 \pm 0.5)\%$.

The track-reconstruction efficiency for charged kaons has been studied in events with similar topology [3] and we use the correction derived therein. The charged-kaon identification efficiency is studied as a function of the track momentum and polar angle using a control sample of kaons from the decay chain $D^{*+} \to \pi^+ D^0, D^0 \to K^-\pi^+$. The ratio of the efficiencies is then used to reweight simulated signal events, resulting in an overall correction that varies slowly from from $-2\%$ at 2.6 GeV/$c^2$ to $-4\%$ at 6 GeV/$c^2$, and then falls to about $-10\%$ at 7.5 GeV/$c^2$. The statistical uncertainty in the correction term defines the systematic uncertainty in this correction.

The remaining criteria are based on $M^2_{\rm miss}$ and $p_{T,K^+K^-}$, which we believe to be well simulated. The track momentum and angular resolutions have been studied in, e.g., Ref. [27] for $e^+e^- \to \mu^+\mu^-\gamma$ events with a detected photon. Based on this and similar variables in our previous ISR studies, we make no correction, and assign a conservative systematic uncertainty of 1.5% to cover these remaining factors. The corrections to the detection efficiency are listed in Table II.

## VI. THE $e^+e^- \to K^+K^-$ CROSS SECTION AND THE CHARGED-KAON FORM FACTOR

The $e^+e^- \to K^+K^-$ cross section in each $K^+K^-$ mass interval $i$ is calculated as

$$\sigma_{K^+K^-,i} = \frac{N_{{\rm sig},i}}{\varepsilon_i L_i}. \tag{7}$$

The number of selected events ($N_{{\rm sig},i}$) for each $K^+K^-$ mass interval after background subtraction is listed in Table III.

TABLE III. The $K^+K^-$ invariant-mass interval ($M_{K^+K^-}$), number of selected events ($N_{\rm sig}$) after background subtraction, detection efficiency ($\varepsilon$), ISR luminosity ($L$), measured $e^+e^- \to K^+K^-$ cross section ($\sigma_{K^+K^-}$), and the charged-kaon form factor ($|F_K|$). For the number of events and cross section, the first uncertainty is statistical and the second is systematic. For the form factor, we quote the combined uncertainty. For the mass interval 7.5–8.0 GeV/$c^2$, the 90% C.L. upper limits for the cross section and form factor are listed.

| $M_{K^+K^-}$ (GeV/$c^2$) | $N_{\rm sig}$ | $\varepsilon$ (%) | $L$ (pb$^{-1}$) | $\sigma_{K^+K^-}$ (pb) | $\lvert F_K\rvert \times 100$ |
|---|---|---|---|---|---|
| 2.6–2.7 | $75 \pm 9 \pm 2$ | 0.96 | 113 | $69.3 \pm 8.1 \pm 3.7$ | $16.7 \pm 1.1$ |
| 2.7–2.8 | $121 \pm 11 \pm 2$ | 1.94 | 118 | $52.9 \pm 4.9 \pm 2.4$ | $15.0 \pm 0.8$ |
| 2.8–2.9 | $157 \pm 13 \pm 2$ | 3.03 | 122 | $42.0 \pm 3.4 \pm 1.6$ | $13.7 \pm 0.6$ |
| 2.9–3.0 | $152 \pm 13 \pm 2$ | 3.69 | 127 | $32.2 \pm 2.7 \pm 1.2$ | $12.4 \pm 0.6$ |
| 3.0–3.2 | $297 \pm 22 \pm 3$ | 5.07 | 271 | $21.7 \pm 1.6 \pm 0.6$ | $10.6 \pm 0.4$ |
| 3.2–3.4 | $279 \pm 17 \pm 2$ | 6.43 | 292 | $14.8 \pm 0.9 \pm 0.4$ | $9.2 \pm 0.3$ |
| 3.4–3.6 | $194 \pm 16 \pm 2$ | 7.81 | 313 | $7.92 \pm 0.63 \pm 0.24$ | $7.1 \pm 0.3$ |
| 3.6–3.8 | $162 \pm 16 \pm 1$ | 9.15 | 336 | $5.26 \pm 0.51 \pm 0.16$ | $6.1 \pm 0.3$ |
| 3.8–4.0 | $152 \pm 13 \pm 1$ | 9.80 | 361 | $4.30 \pm 0.36 \pm 0.13$ | $5.7 \pm 0.3$ |
| 4.0–4.2 | $105 \pm 11 \pm 1$ | 10.8 | 386 | $2.52 \pm 0.25 \pm 0.08$ | $4.60 \pm 0.25$ |
| 4.2–4.4 | $81 \pm 9 \pm 1$ | 11.0 | 413 | $1.79 \pm 0.20 \pm 0.06$ | $4.05 \pm 0.25$ |
| 4.4–4.6 | $44.7 \pm 6.9 \pm 0.6$ | 11.9 | 442 | $0.85 \pm 0.13 \pm 0.03$ | $2.91 \pm 0.23$ |
| 4.6–4.8 | $41.2 \pm 6.6 \pm 0.3$ | 12.5 | 473 | $0.70 \pm 0.11 \pm 0.03$ | $2.74 \pm 0.23$ |
| 4.8–5.0 | $36.2 \pm 6.2 \pm 0.5$ | 13.1 | 507 | $0.55 \pm 0.09 \pm 0.02$ | $2.52 \pm 0.22$ |
| 5.0–5.2 | $26.8 \pm 5.3 \pm 0.3$ | 12.9 | 543 | $0.38 \pm 0.08 \pm 0.02$ | $2.19 \pm 0.22$ |
| 5.2–5.5 | $45.2 \pm 6.9 \pm 0.6$ | 14.4 | 888 | $0.35 \pm 0.05 \pm 0.01$ | $2.21 \pm 0.18$ |
| 5.5–6.0 | $34.6 \pm 6.6 \pm 0.7$ | 13.5 | 1710 | $0.150 \pm 0.029 \pm 0.006$ | $1.54 \pm 0.15$ |
| 6.0–6.5 | $10.7 \pm 4.5 \pm 1.2$ | 10.6 | 2062 | $0.049 \pm 0.021 \pm 0.006$ | $0.95 \pm 0.22$ |
| 6.5–7.0 | $13.6 \pm 5.3 \pm 0.7$ | 11.6 | 2523 | $0.047 \pm 0.018 \pm 0.004$ | $1.00 \pm 0.20$ |
| 7.0–7.5 | $7.4 \pm 5.3 \pm 1.9$ | 11.9 | 3144 | $0.020 \pm 0.014 \pm 0.004$ | $0.70^{+0.23}_{-0.36}$ |
| 7.5–8.0 | $0.0 \pm 6.9 \pm 2.0$ | 9.36 | 4015 | $< 0.024$ | $< 0.9$ |

The $N_{\rm sig}$ values for $M_{K^+K^-} > 5.5$ GeV/$c^2$ differ from the corresponding values in Table I. They are corrected to correspond to the nominal selection $|M^2_{\rm miss}| < 1$ GeV$^2/c^4$ as described in Sec. IV A. The first uncertainty in $N_{\rm sig}$ is statistical; the second is systematic due to background subtraction. The value of the ISR luminosity $L_i$ is obtained by integrating $W(s,x)$ from Refs. [12,13] over mass interval $i$ and is listed in Table III. The formulas from Refs. [12,13] include higher-order radiative corrections. However, we do not include in $W(s,x)$ corrections for leptonic and hadronic vacuum polarization in the photon propagator. Cross sections obtained in this way are referred to as "dressed."

The values obtained for the $e^+e^- \to K^+K^-$ cross section are listed in Table III. For the mass intervals 3.0–3.2 GeV/$c^2$ and 3.6–3.8 GeV/$c^2$ we quote the nonresonant cross sections with the respective $J/\psi$ and $\psi(2S)$ contributions excluded. The quoted uncertainties are statistical and systematic, respectively. The statistical uncertainty results from the statistical uncertainty in the number of selected $K^+K^-\gamma$ events. The systematic uncertainty includes the systematic uncertainty in the number of events, the statistical uncertainty in the detection efficiency (1.5%–4.0%), and the uncertainties in the efficiency correction (2.6%–5.1%), the integrated luminosity (0.5%) [19], and the ISR luminosity (0.5%) [12,13]. For the mass interval 7.5–8.0 GeV/$c^2$, the 90% confidence level (C.L.) upper limit on the cross section is listed. The measured cross section is shown in Fig. 10.

It is more convenient to perform comparisons with previous measurements and theoretical predictions in terms of the form factor. The values of the charged-kaon electromagnetic form factor obtained using Eq. (3) are listed in Table III. The form factor is plotted in Fig. 11 as a function of $M_{K^+K^-}$ over the range 2.6–5.0 GeV/$c^2$, together with all

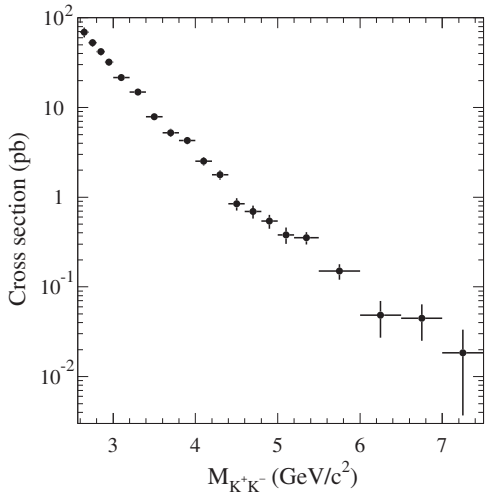


FIG. 10. The $e^+e^- \to K^+K^-$ cross section measured in this work.

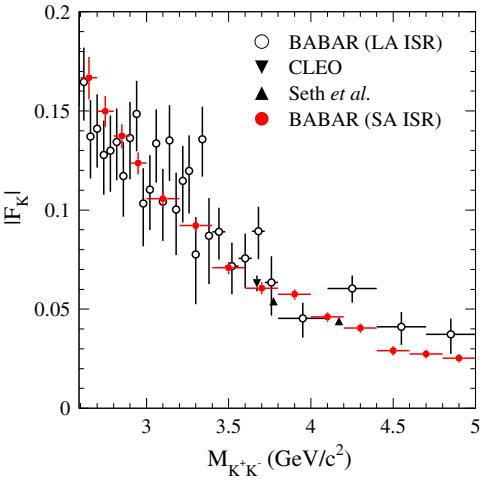


FIG. 11 (color online). The charged-kaon electromagnetic form factor measured in this analysis [*BABAR* (SA ISR)] in comparison with previous measurements: CLEO [8], Seth *et al.* [9], and *BABAR* (LA ISR) [3] in the mass region 2.6–5.0 GeV/$c^2$. Only statistical uncertainties are shown.

other measurements [3,8,9]. The present measurement is consistent within the uncertainties with our previous, independent LA ISR result [3], which used a data sample corresponding only to 232 fb$^{-1}$, and provides a much better constraint on the mass dependence in this region.

To compare our results with the precise measurements of Refs. [8,9], we plot in Fig. 12 the scaled form factor $M^2_{K^+K^-}|F_K(M_{K^+K^-})|$ and fit our data with a smooth

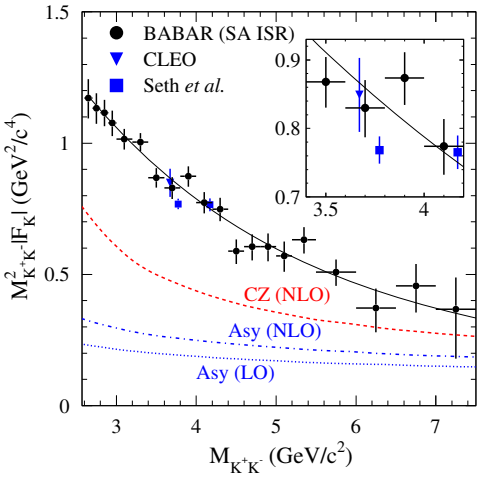


FIG. 12 (color online). The scaled charged-kaon electromagnetic form factor measured in this analysis [*BABAR* (SA ISR)] and in other experiments: CLEO [8] and Seth *et al.* [9]. Our data are approximated by a smooth curve. The dotted blue curve shows the LO pQCD prediction for the form factor obtained with the asymptotic kaon distribution amplitude. The dot-dashed blue and dashed red curves are the NLO pQCD predictions obtained with the asymptotic and Chernyak-Zhitnitsky distribution amplitudes, respectively. The inset shows an enlarged version of the mass region 3.4–4.2 GeV/$c^2$.

function $x^2|F_K(x)| = A/(x^\gamma + B)$, where $A$, $B$, and $\gamma$ are fitted parameters. As seen in the inset, the CLEO and Seth *et al.* points at 3.67 and 4.17 GeV/$c^2$, respectively, are consistent with this function, whereas the Seth *et al.* point at 3.772 GeV/$c^2$ lies about three standard deviations below. Since this data point is obtained at the maximum of the $\psi(3770)$ resonance, the deviation may be a result of interference between the resonant and nonresonant amplitudes of the $e^+e^- \to K^+K^-$ reaction, which we discuss in the next section.

The dotted curve in Fig. 12 represents the leading-order (LO) asymptotic pQCD prediction of Eq. (1), calculated with $\alpha_s(M^2_{K^+K^-}/4)$ [29]. It lies well below most of the data, which might be explained by higher-order pQCD, power corrections, and a deviation of the kaon distribution amplitude (DA), which describes the quark relative momentum distribution inside the meson, from its asymptotic shape. The dot-dashed curve represents the leading-twist, next-to-leading-order (NLO) prediction using the asymptotic DA, obtained by multiplying the pion form factor from Ref. [29] by a factor $f_K^2/f_\pi^2 \approx 1.45$. The NLO correction leads to an increase of about 20%, nearly independent of mass. The dashed curve represents the NLO prediction using the Chernyak-Zhitnitsky (CZ) DA, obtained by multiplying the result in Ref. [29] by a factor of 0.95 [30].

Our data lie well above all predictions. However, they decrease faster than $\alpha_s/M^2_{K^+K^-}$ as $M_{K^+K^-}$ increases, and are consistent with an approach to the pQCD prediction at higher mass. In particular, the ratio of the measured form factor to the asymptotic pQCD prediction (curve Asy(LO) in Fig. 12) changes from about 5.3 at 3 GeV/$c^2$ to about 2.6 at 7 GeV/$c^2$.

## VII. $J/\psi$ AND $\psi(2S)$ DECAYS INTO $K^+K^-$

To study the production of $K^+K^-$ pairs through the $J/\psi$ and $\psi(2S)$ resonances, we increase the detection efficiency by selecting events with the looser requirements $p_{T,K^+K^-} < 1$ GeV/$c$ and $-2 < M^2_{\rm miss} < 3$ GeV$^2/c^4$. The resulting $K^+K^-$ mass spectra in the $J/\psi$ and $\psi(2S)$ mass regions are shown in Fig. 13. Each of these spectra is fitted with the sum of a signal probability density function (PDF) and a linear background. The signal PDF is a Breit-Wigner (BW) function convolved with a double-Gaussian function describing signal resolution. In each fit, the BW mass and width are fixed to their known values [11] and the nominal resolution parameters are taken from simulation. In order to account for deficiencies in the simulation, a mass shift $\Delta M$ is allowed, and an increase in both Gaussian widths by a term $\sigma_G$ added in quadrature is introduced. The free parameters in the $J/\psi$ fit are the numbers of signal and background events, the slope of the background function, $\Delta M$, and $\sigma_G$. In the $\psi(2S)$ fit, $\sigma_G$ and $\Delta M$ are fixed to the values obtained for the $J/\psi$.

The fitted curves are shown in Fig. 13. The numbers of $J/\psi$ and $\psi(2S)$ events are found to be $462 \pm 28$ and $66 \pm 13$, respectively. Results for other fitted parameters are $\sigma_G = 3 \pm 3$ MeV/$c^2$ and $\Delta M = M_{J/\psi} - M^{\rm MC}_{J/\psi} = (0.0 \pm 0.9)$ MeV/$c^2$. The $\sigma_G$ value corresponds to a difference of about 4% in mass resolution (11 MeV/$c^2$ at the $J/\psi$) between data and simulation. The detection efficiencies, corrected for the data-MC simulation difference in detector response, are $(7.6 \pm 0.2)\%$ for the $J/\psi$ and $(13.4 \pm 0.3)\%$ for the $\psi(2S)$.

The total cross sections for the processes $e^+e^- \to \psi\gamma \to K^+K^-\gamma$, where $\psi$ is a narrow resonance like the $J/\psi$ or $\psi(2S)$, is proportional to the electronic width of the resonance and its branching fraction into $K^+K^-$, i.e., $\sigma_{\psi\gamma} = a_\psi \Gamma(\psi \to e^+e^-)B(\psi \to K^+K^-)$. The coefficient $a_\psi$ can be calculated by integrating Eq. (2) with $\sigma_{K^+K^-}$ set to the appropriate BW function. Using $W(s,x)$ from Refs. [12,13], we obtain $a_{J/\psi} = 6.91$ nb/keV and $a_{\psi(2S)} = 6.07$ nb/keV.

From the measured values of the cross sections, $\sigma^{\rm exp}_{\psi\gamma} = N_\psi/(\varepsilon L)$, we obtain the measured values of the products $\Gamma(\psi \to e^+e^-)\mathcal{B}(\psi \to K^+K^-)$ listed in Table IV. The term "measured value" is used because the value of the product obtained in this way may differ from the true value

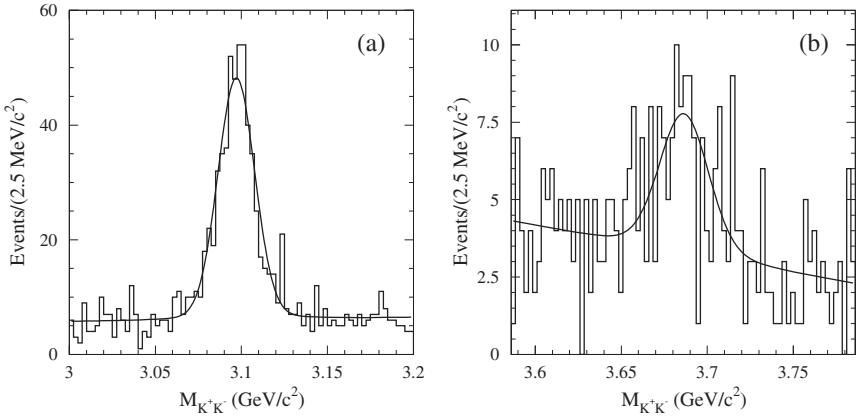


FIG. 13. The $K^+K^-$ mass spectra in the regions near the $J/\psi$ (a) and $\psi(2S)$ (b) resonances. The curves exhibit the results of the fits described in the text.

TABLE IV. The products $\Gamma(\psi \to e^+e^-)\mathcal{B}(\psi \to K^+K^-)$ and the branching fractions $\mathcal{B}(\psi \to K^+K^-)$ obtained in this work for the $J/\psi$ and $\psi(2S)$ resonances. The directly measured values are shown in the rows labeled "measured values." In the rows marked as "corrected," the values of the products and branching fractions corrected for the shift due to interference between resonant and nonresonant amplitudes are listed for opposite signs of $\sin\varphi$. In the row marked "$e^+e^- \to K^+K^-$ average," we give the average of the values of the branching fractions measured in the reaction $e^+e^- \to K^+K^-$. In the row "$\psi(2S) \to J/\psi\pi^+\pi^-$, $J/\psi \to K^+K^-$", the result for the $J/\psi \to K^+K^-$ branching fraction obtained in Ref. [18] is reported.

| $\Gamma(\psi \to e^+e^-)\mathcal{B}(\psi \to K^+K^-)$ (eV) | $J/\psi$ | $\psi(2S)$ |
|---|---|---|
| Measured value | $1.86 \pm 0.11 \pm 0.05$ | $0.173 \pm 0.035 \pm 0.005$ |
| Corrected with $\sin\varphi > 0$ | $1.78 \pm 0.11 \pm 0.05$ | $0.147 \pm 0.035 \pm 0.005$ |
| Corrected with $\sin\varphi < 0$ | $1.94 \pm 0.11 \pm 0.05$ | $0.197 \pm 0.035 \pm 0.005$ |
| $\mathcal{B}(\psi \to K^+K^-) \times 10^4$ | $J/\psi$ | $\psi(2S)$ |
| Measured value | $3.36 \pm 0.20 \pm 0.12$ | $0.73 \pm 0.15 \pm 0.02$ |
| Corrected with $\sin\varphi > 0$ | $3.22 \pm 0.20 \pm 0.12$ | $0.62 \pm 0.15 \pm 0.02$ |
| Corrected with $\sin\varphi < 0$ | $3.50 \pm 0.20 \pm 0.12$ | $0.83 \pm 0.15 \pm 0.02$ |
| $e^+e^- \to K^+K^-$ average | $2.43 \pm 0.26$ [3,31,32] | $0.71 \pm 0.05$ [11] |
| $\psi(2S) \to J/\psi\pi^+\pi^-$, $J/\psi \to K^+K^-$ [18] | $2.86 \pm 0.21$ | |

due to interference with the nonresonant process $e^+e^- \to K^+K^-$, as discussed below. The quoted systematic uncertainty includes the uncertainties in the detection efficiency, the integrated luminosity (0.5%), and the theoretical uncertainty in the ISR luminosity (0.5%). Using the nominal values of the electronic widths [11], $\Gamma(J/\psi \to e^+e^-) = 5.55 \pm 0.14$ keV and $\Gamma(\psi(2S) \to e^+e^-) = 2.37 \pm 0.04$ keV, we calculate the measured values of the $\psi \to K^+K^-$ branching fractions listed in Table IV. Since the decay $\psi(2S) \to K^+K^-$ was studied previously only in the reaction $e^+e^- \to K^+K^-$, our measurement of $\mathcal{B}(\psi(2S) \to K^+K^-)$ can be directly compared with the PDG value [11], $(0.71 \pm 0.05) \times 10^{-4}$. Although it is less precise, our measured value agrees well with that from Ref. [11]. For $J/\psi \to K^+K^-$ there are several measurements [3,31,32] in the $e^+e^- \to K^+K^-$ reaction, and one measurement [18] in which $J/\psi$'s were produced in the $\psi(2S) \to J/\psi\pi^+\pi^-$ decay. To compare with the $e^+e^-$ measurements, we calculate the average of the results [3,31,32], and obtain the value $(2.43 \pm 0.26) \times 10^{-4}$. Our result is larger than this average by 2.7 standard deviations. A comparison with the measurement of Ref. [18] is presented below after applying a correction for interference.

To estimate the effect of interference, we represent the c.m. energy ($E$) dependence of the $e^+e^- \to K^+K^-$ cross section near the $\psi$ resonance as [33]

$$\begin{aligned}\sigma_{K^+K^-}(E) &= \sigma_0\left|1-\sqrt{\frac{\sigma_\psi}{\sigma_0}}(A_\gamma + A_s e^{i\varphi})\frac{m\Gamma}{D}\right|^2 \\ &= \sigma_0 + \sigma_\psi\left[\mathcal{B}(\psi \to K^+K^-) + 2\sqrt{\frac{\sigma_0}{\sigma_\psi}}A_s\sin\varphi\right] \\ &\times\frac{m^2\Gamma^2}{|D|^2} - 2\sqrt{\sigma_0\sigma_\psi}(A_\gamma + A_s\cos\varphi)\frac{m\Gamma(m^2-E^2)}{|D|^2},\end{aligned} \tag{8}$$

where $\sigma_0$ is the nonresonant cross section [Eq. (3)], $\sigma_\psi = (12\pi/m^2)\mathcal{B}(\psi \to e^+e^-)$, $A_\gamma$ and $A_s$ are the moduli of the single-photon and strong $\psi$ decay amplitudes, respectively, $\varphi$ is their relative phase, $D = m^2 - E^2 - im\Gamma$, and $m$ and $\Gamma$ are the resonance mass and width, respectively. The decay amplitudes are defined such that $\mathcal{B}(\psi \to K^+K^-) = |A_\gamma + A_s e^{i\varphi}|^2$. The value of the single-photon contribution is related to the kaon form factor through

$$A_\gamma^2 = \mathcal{B}(\psi \to e^+e^-)\frac{|F_K(m)|^2}{4}\beta^3(m), \tag{9}$$

where $\beta$ is the phase-space factor from Eq. (3).

For narrow resonances, the interference term proportional to $m^2 - E^2$ integrates to zero due to the beam energy spread in direct $e^+e^-$ experiments and detector resolution in ISR measurements. The remaining interference term has a BW shape and causes a shift of the measured $\mathcal{B}(\psi \to K^+K^-)$ relative to its true value by

$$\delta\mathcal{B} = 2\sqrt{\frac{\sigma_0}{\sigma_\psi}}A_s\sin\varphi. \tag{10}$$

The values of $\cos\varphi$ and $A_s$ can be obtained from a combined analysis of the $\psi \to K^+K^-$ and $\psi \to K_SK_L$ decays, whose branching fractions depend on the same strong amplitude [16,17]

$$\begin{aligned}\mathcal{B}(\psi \to K^+K^-) &= |A_\gamma^{K^+K^-} + A_s e^{i\varphi}|^2, \\ \mathcal{B}(\psi \to K_SK_L) &= |\kappa A_\gamma^{K^+K^-} + A_s e^{i\varphi}|^2,\end{aligned} \tag{11}$$

where $\kappa$ is the ratio of the single-photon amplitudes for the $\psi \to K_SK_L$ and $\psi \to K^+K^-$ decays, and $|\kappa| = A_\gamma^{K_SK_L}/A_\gamma^{K^+K^-}$. It is expected that in the energy region under study,

the single-photon amplitudes have the same sign of the real parts, and similar ratios of the imaginary-to-real parts [34]; i.e., $\kappa$ is a positive real number to a good approximation.

For the branching fraction $\mathcal{B}(J/\psi \to K^+K^-)$ in Eqs. (11), we use the average of the existing measurements 3,18,31,32]] and our result. For $\mathcal{B}(J/\psi \to K_SK_L)$ there are two relatively precise measurements, $(1.82 \pm 0.14) \times 10^{-4}$ [35] and $(2.62 \pm 0.21) \times 10^{-4}$ [18], which are not consistent with each other. We solve Eqs. (11) separately for these two values of $\mathcal{B}(J/\psi \to K_SK_L)$. The branching fractions measured in the reactions $e^+e^- \to K^+K^-$ and $e^+e^- \to K_SK_L$ are corrected as $\mathcal{B} \to \mathcal{B} - \delta\mathcal{B}$ before averaging, where $\delta\mathcal{B}$ is given by Eq. (10). This correction is not needed for the measurements of Ref. [18], in which the $J/\psi$ mesons are produced in $\psi(2S) \to J/\psi\pi^+\pi^-$ decays. For $\psi(2S)$ decays we use the branching fraction values from Ref. [11] corrected using Eq. (10).

The coefficient $|\kappa|$ in Eqs. (11) is equal to the ratio of the neutral- and charged-kaon form factors $|F_{K^0}/F_K|$. Data on $F_{K^0}$ above 2 GeV are scarce. There are two measurements [5,36] near 2 GeV, from which we estimate $|\kappa| = 0.28 \pm 0.08$, and there is only one measurement at higher energy, namely $|\kappa| = 0.12 \pm 0.04$ at 4.17 GeV [37]. Using linear interpolation we estimate $|\kappa| = 0.2 \pm 0.1$ at the mass of the $J/\psi$ and $0.15 \pm 0.07$ at the mass of the $\psi(2S)$. The values of the charged-kaon form factor, $F_K(M_{J/\psi}) = 0.107 \pm 0.002$ and $F_K(M_{\psi(2S)}) = 0.0634 \pm 0.0014$, needed to calculate $A_\gamma^{K^+K^-}$, are taken from the fit to our form factor data shown in Fig. 12.

The values of $\varphi$ and $\delta\mathcal{B}(\psi \to K^+K^-)$ obtained using Eqs. (10) and (11) are listed in Tables V and VI. Since Eqs. (11) do not allow us to determine the sign of $\sin\varphi$, the calculations are performed twice, once assuming $\sin\varphi > 0$ and once assuming $\sin\varphi < 0$. For the results in Table V the two upper (bottom) rows marked "BES" ("Seth *et al.*") present results obtained using $\mathcal{B}(J/\psi \to K_SK_L)$ from Ref. [35] (Ref. [18]). We also list the results obtained for $\kappa = 0$, corresponding to the assumption $A_\gamma^{K_SK_L} \ll A_\gamma^{K^+K^-}$ used for most previous determinations of $\varphi$. It is seen that allowing $A_\gamma^{K_SK_L}$ to be nonzero does not lead to a significant change in the results.

TABLE V. The relative phase ($\varphi$) between the single-photon and strong amplitudes for $J/\psi \to K\bar{K}$ decays calculated with $\kappa = A_\gamma^{K_SK_L}/A_\gamma^{K^+K^-} = 0.2 \pm 0.1$ and $\kappa = 0$, and the correction to the value of $\mathcal{B}(J/\psi \to K^+K^-)$ measured in the reaction $e^+e^- \to K^+K^-$. The calculation is performed for the value of $\mathcal{B}(J/\psi \to K_SK_L)$ obtained in Ref. [35], the value obtained in Ref. [18], and assuming either a positive or negative value for $\sin\varphi$.

| $J/\psi \to K_SK_L$ | $\varphi$ | $\varphi(\kappa = 0)$ | $\delta\mathcal{B}(J/\psi \to K^+K^-) \times 10^4$ |
|---|---|---|---|
| BES [35] | $(97 \pm 5)^\circ$ | $(98 \pm 4)^\circ$ | $0.13 \pm 0.01$ |
| | $-(97 \pm 5)^\circ$ | $-(96 \pm 4)^\circ$ | $-0.13 \pm 0.01$ |
| Seth *et al.* [18] | $(111 \pm 5)^\circ$ | $(108 \pm 4)^\circ$ | $0.15 \pm 0.01$ |
| | $-(109 \pm 5)^\circ$ | $-(107 \pm 4)^\circ$ | $-0.15 \pm 0.01$ |

TABLE VI. The relative phase ($\varphi$) between the single-photon and strong amplitudes for $\psi(2S) \to K\bar{K}$ decays calculated with $\kappa = A_\gamma^{K_SK_L}/A_\gamma^{K^+K^-} = 0.15 \pm 0.07$ and $\kappa = 0$, and the correction to the value of $\mathcal{B}(\psi(2S) \to K^+K^-)$ measured in the reaction $e^+e^- \to K^+K^-$. The calculation was performed for each sign of $\sin\varphi$.

| $\varphi$ | $\varphi(\kappa = 0)$ | $\delta\mathcal{B}(\psi(2S) \to K^+K^-) \times 10^4$ |
|---|---|---|
| $(82 \pm 12)^\circ$ | $(92 \pm 9)^\circ$ | $0.11 \pm 0.01$ |
| $-(58 \pm 14)^\circ$ | $-(57 \pm 12)^\circ$ | $-0.10 \pm 0.02$ |

For the $J/\psi$, for which the most precise measurement of $\mathcal{B}(J/\psi \to K^+K^-)$ was performed in $\psi(2S)$ decay, the result for $\cos\varphi$ is weakly dependent on the sign of $\sin\varphi$. We confirm the conclusion of Refs. [16,17] to the effect that the strong amplitude describing $J/\psi \to K^+K^-$ decay has a large imaginary part. Using $\mathcal{B}(J/\psi \to K_SK_L)$ from Ref. [18], a non-negligible real part of the strong amplitude is obtained.

For the $\psi(2S)$, the result on $\cos\varphi$ is strongly dependent on the sign of $\sin\varphi$. Here theoretical arguments may help to choose the sign. The ratio of the strong amplitudes for $\psi(2S) \to K\bar{K}$ and $J/\psi \to K\bar{K}$ decays is expected [38] to be

$$\frac{A_s^2(\psi(2S) \to K\bar{K})}{A_s^2(J/\psi \to K\bar{K})} \approx \frac{\mathcal{B}(\psi(2S) \to e^+e^-)}{\mathcal{B}(J/\psi \to e^+e^-)} \frac{\beta^3(M_{\psi(2S)})}{\beta^3(M_{J/\psi})} = 0.138 \pm 0.003. \quad (12)$$

The experimental value of this ratio (for $J/\psi$ we used $A_s$ obtained with $\mathcal{B}(J/\psi \to K_SK_L)$ from Ref. [18]) is $0.192 \pm 0.026$ for $\sin\varphi < 0$ and $0.170 \pm 0.023$ for $\sin\varphi > 0$. The result for the positive sign is in slightly better agreement with the prediction.

Using the values of $\delta\mathcal{B}$ given in Tables V and VI, we correct the measured values of the products $\Gamma(\psi \to e^+e^-)\mathcal{B}(\psi \to K^+K^-)$ and the branching fractions and list the corrected values in Table IV.

The corrected values of $\mathcal{B}(J/\psi \to K^+K^-)$ can be compared with the measurement of Ref. [18] $(2.86 \pm 0.21) \times 10^{-4}$. The difference between the two measurements is $2\sigma$ for $\sin\varphi < 0$, and $1\sigma$ for $\sin\varphi > 0$. Our result for $J/\psi \to K^+K^-$ thus provides an indication that $\sin\varphi$ is positive. It should be stressed that the shifts we find between the measured and true values of $\mathcal{B}(\psi \to K^+K^-)$ are significant: about 5% for the $J/\psi$ and about 15% for the $\psi(2S)$. Thus, the interference effect should be taken into account in any future precise measurements of the branching fraction for $J/\psi \to K^+K^-$ or $\psi(2S) \to K^+K^-$.

## VIII. SUMMARY

The process $e^+e^- \to K^+K^-\gamma$ has been studied in the $K^+K^-$ invariant mass range from 2.6 to 8 GeV/$c^2$ using events in which the photon is emitted close to the collision axis. From the measured $K^+K^-$ mass spectrum we obtain the $e^+e^- \to K^+K^-$ cross section and determine the charged-kaon electromagnetic form factor (Table III). This is the first measurement of the kaon form factor for $K^+K^-$ invariant masses higher than 5 GeV/$c^2$ and the most precise measurement in the range 2.6–5.0 GeV/$c^2$. Our data indicate clearly that the difference between the measured form factor and the leading twist pQCD prediction decreases with increasing $K^+K^-$ invariant mass.

We present measurements of the $J/\psi \to K^+K^-$ and $\psi(2S) \to K^+K^-$ branching fractions (Table IV). Using the measured values of the branching fractions and charged-kaon form factors, and data from other experiments on $e^+e^- \to K_SK_L$ and $\psi \to K\bar{K}$ decays, we have determined the phase difference $\varphi$ between the strong and single-photon amplitudes for $J/\psi \to K\bar{K}$ and $\psi(2S) \to K\bar{K}$ decays. We have calculated the shifts in the measured values of the branching fractions due to interference between resonant and nonresonant amplitudes in the $e^+e^- \to K^+K^-$ reaction. The shift has been found to be relatively large, about $\pm 5\%$ for the $J/\psi$ and about $\pm 15\%$ for the $\psi(2S)$, where the sign is determined by the sign of $\sin\varphi$.

It should be noted that the sign of $\sin\varphi$ for $J/\psi$ decays can be determined experimentally from the difference, $\delta\mathcal{B}/\mathcal{B}$, between the $J/\psi \to K^+K^-$ branching fractions measured in the reaction $e^+e^- \to K^+K^-$ and in the decay $\psi(2S) \to J/\psi\pi^+\pi^-$. We hope that this measurement will be performed in future experiments.

## ACKNOWLEDGMENTS

We thank V. L. Chernyak for useful discussions. We are grateful for the extraordinary contributions of our PEP-II2 colleagues in achieving the excellent luminosity and machine conditions that have made this work possible. The success of this project also relies critically on the expertise and dedication of the computing organizations that support *BABAR*. The collaborating institutions wish to thank SLAC for its support and the kind hospitality extended to them. This work is supported by the U.S. Department of Energy and National Science Foundation, the Natural Sciences and Engineering Research Council (Canada), the Commissariat à l'Energie Atomique and Institut National de Physique Nucléaire et de Physique des Particules (France), the Bundesministerium für Bildung und Forschung and Deutsche Forschungsgemeinschaft (Germany), the Istituto Nazionale di Fisica Nucleare (Italy), the Foundation for Fundamental Research on Matter (Netherlands), the Research Council of Norway, the Ministry of Education and Science of the Russian Federation, Ministerio de Economía y Competitividad (Spain), the Science and Technology Facilities Council (United Kingdom), and the Binational Science Foundation (U.S.-Israel). Individuals have received support from the Marie-Curie IEF program (European Union) and the A. P. Sloan Foundation (USA).

[1] M. N. Achasov *et al.* (SND Collaboration), Phys. Rev. D **63**, 072002 (2001).
[2] R. R. Akhmetshin *et al.* (CMD-2 Collaboration), Phys. Lett. B **669**, 217 (2008).
[3] J. P. Lees *et al.* (*BABAR* Collaboration), Phys. Rev. D **88**, 032013 (2013).
[4] P. M. Ivanov, L. M. Kurdadze, M. Yu. Lelchuk, V. A. Sidorov, A. N. Skrinsky, A. G. Chilingarov, Yu. M. Shatunov, B. A. Shwartz, and S. I. Eidelman, Phys. Lett. **107B**, 297 (1981); JETP Lett. **36**, 112 (1982).
[5] B. Delcourt, D. Bisello, J.-C. Bizot, J. Buon, A. Cordier, and F. Mané, Phys. Lett. **99B**, 257 (1981); F. Mané, D. Bisello, J.-C. Bizot, J. Buon, A. Cordier, and B. Delcourt, Phys. Lett. **99B**, 261 (1981).
[6] D. Bisello *et al.* (DM2 Collaboration), Z. Phys. C **39**, 13 (1988).
[7] M. N. Achasov *et al.* (SND Collaboration), Phys. Rev. D **76**, 072012 (2007).
[8] T. K. Pedlar *et al.* (CLEO Collaboration), Phys. Rev. Lett. **95**, 261803 (2005).
[9] K. K. Seth, S. Dobbs, Z. Metreveli, A. Tomaradze, T. Xiao, and G. Bonvicini, Phys. Rev. Lett. **110**, 022002 (2013).
[10] V. L. Chernyak, A. R. Zhitnitsky, and V. G. Serbo, JETP Lett. **26**, 594 (1977); G. P. Lepage and S. J. Brodsky, Phys. Lett. **87B**, 359 (1979).
[11] K. A. Olive *et al.* (Particle Data Group), Chin. Phys. C **38**, 090001 (2014).
[12] O. Nicrosini and L. Trentadue, Phys. Lett. B **196**, 551 (1987).
[13] F. A. Berends, W. L. van Neerven, and G. J. H. Burgers, Nucl. Phys. **B297**, 429 (1988); **304**, 921(E) (1988).
[14] M. Benayoun, S. I. Eidelman, V. N. Ivanchenko, and Z. K. Silagadze, Mod. Phys. Lett. A **14**, 2605 (1999).
[15] A. Hoefer, J. Gluza, and F. Jegerlehner, Eur. Phys. J. C **24**, 51 (2002).
[16] M. Suzuki, Phys. Rev. D **60**, 051501 (1999).
[17] J. L. Rosner, Phys. Rev. D **60**, 074029 (1999).
[18] Z. Metreveli, S. Dobbs, A. Tomaradze, T. Xiao, K. K. Seth, J. Yelton, D. M. Asner, G. Tatishvili, and G. Bonvicini, Phys. Rev. D **85**, 092007 (2012).

[19] J. P. Lees *et al.* (*BABAR* Collaboration), Nucl. Instrum. Methods Phys. Res., Sect. A **726**, 203 (2013).
[20] B. Aubert *et al.* (*BABAR* Collaboration), Nucl. Instrum. Methods Phys. Res., Sect. A **479**, 1 (2002); **729**, 615 (2013).
[21] H. Czyz, A. Grzelinska, J. H. Kühn, and G. Rodrigo, Eur. Phys. J. C **39**, 411 (2005).
[22] S. Jadach, W. Placzek, and B. F. L. Ward, Phys. Lett. B **390**, 298 (1997).
[23] B. Aubert *et al.* (*BABAR* Collaboration), Phys. Rev. D **81**, 092003 (2010).
[24] T. Sjöstrand, Comput. Phys. Commun. **82**, 74 (1994).
[25] S. Agostinelli *et al.* (Geant4 Collaboration), Nucl. Instrum. Methods Phys. Res., Sect. A **506**, 250 (2003).
[26] See Supplemental Material at http://link.aps.org/supplemental/10.1103/PhysRevD.92.072008 for the mass spectrum with finer binning in the region of the charmonium resonances $3.0-4.5$ GeV$/c^2$
[27] J. P. Lees *et al.* (*BABAR* Collaboration), Phys. Rev. D **87**, 092005 (2013).
[28] J. P. Lees *et al.* (*BABAR* Collaboration), Phys. Rev. D **88**, 072009 (2013).
[29] B. Melic, B. Nizic, and K. Passek, Phys. Rev. D **60**, 074004 (1999).
[30] V. L. Chernyak and A. R. Zhitnitsky, Phys. Rep. **112**, 173 (1984).
[31] R. Brandelik *et al.* (DASP Collaboration), Z. Phys. C **1**, 233 (1979).
[32] R. M. Baltrusaitis *et al.* (Mark III Collaboration), Phys. Rev. D **32**, 566 (1985).
[33] R. Gatto, Nuovo Cimento **28**, 658 (1963).
[34] V. L. Chernyak (private communication).
[35] J. Z. Bai *et al.* (BES Collaboration), Phys. Rev. D **69**, 012003 (2004).
[36] J. P. Lees *et al.* (*BABAR* Collaboration), Phys. Rev. D **89**, 092002 (2014).
[37] K. K. Seth, S. Dobbs, A. Tomaradze, T. Xiao, and G. Bonvicini, Phys. Lett. B **730**, 332 (2014).
[38] T. Appelquist and H. D. Politzer, Phys. Rev. Lett. **34**, 43 (1975).